Nanoindentation of ion-implanted crystalline germanium

D. J. Oliver,[1,*] S. Ruffell,[2] J. E. Bradby,[2] J. S. Williams,[2] M. V. Swain,[3] P. Munroe,[4] and P. J. Simpson[5]
[1]*Department of Physics, McGill University, Montréal, Quebec, Canada H3A 2T8*
[2]*Department of Electronic Materials Engineering, Research School of Physics and Engineering, The Australian National University, Canberra, Australian Capital Territory 0200, Australia*
[3]*Biomaterials Science Research Unit, Faculty of Dentistry, The University of Sydney, Eveleigh, New South Wales 1430, Australia*
[4]*Electron Microscope Unit, University of New South Wales, Sydney, New South Wales 2052, Australia*
[5]*Department of Physics and Astronomy, University of Western Ontario, London, Ontario, Canada N6A 3K7*
(Received 26 March 2009; revised manuscript received 10 August 2009; published 22 September 2009)

Most indentation studies to date on crystalline germanium (c-Ge) and related covalent semiconductors have been carried out on pristine defect-free material. This paper addresses the paucity of studies on imperfect crystalline materials by exploring the impact of defects generated by ion implantation, prior to contact damage, upon the mechanical properties of c-Ge. Implantation with Ge ions is carried out to generate a layer of highly defective but still-crystalline Ge. Under nanoindentation with a sharp diamond tip, enhanced plasticity is observed relative to pristine material. Characterization by cross-sectional transmission electron microscopy, atomic force microscopy, and load curve analysis shows softening, quasiductile extrusion, and cracking suppression taking place. These changes can be explained by the high density of defects, and dangling bonds in particular, created by ion implantation and revealed by positron-annihilation spectroscopy, and are proportional to the fraction of "missing bonds" or vacancies in the material. A thermal annealing step at 200 °C is sufficient to restore the mechanical response of pristine material, despite incomplete recovery of the original pristine crystal structure.

DOI: 10.1103/PhysRevB.80.115210 PACS number(s): 61.82.Fk, 62.20.F−

I. INTRODUCTION

Nanoindentation with a sharp diamond tip is a powerful tool for investigating the mechanical behavior of hard covalent materials. Crystalline Ge (c-Ge) is a semiconductor material with important technological applications in electronics and is now integrated into silicon devices and circuits to improve carrier mobility and ultimately device and circuit speed.[1,2] Germanium is mechanically softer than silicon and the strain introduced by integration of c-Ge layers with silicon raises issues over its mechanical stability. Understanding its mechanical properties is thus crucial not only in the final device structure but also for handling and machining during device fabrication.[3] As an elemental covalent solid of similar diamond cubic structure to silicon it is also an ideal material for comparing its mechanical behavior and mechanisms for deformation with those of silicon that have been much more extensively studied. The response of c-Ge to nanoindentation has been investigated by several groups. Although there have been some suggestions that a pressure-induced phase transformation takes place,[4,5] it appears that instead under most loading conditions the dominant deformation mechanisms in Ge during nanoindentation are shear-induced slip and twinning.[6–9] Most nanoindentation studies into the mechanical properties of c-Ge,[4–9] and also silicon (Si) and compound semiconductors,[4,6,10–13] have been carried out on pristine defect-free single crystals. This raises the question of how the presence of pre-existing defects in the crystalline structure affects the mechanical response of a covalent material. In most materials the presence of defects impedes slip, raising the mechanical hardness through work hardening.[14,15] However, in covalent crystals, hardness has been regarded as an intrinsic material property. Recent theoretical treatments by Gao and others[16–18] have argued hardness in these materials is dependent on bond strength and density and independent of extrinsic factors such as the defect state. Since Ge is now an important material in modern silicon-based circuits where implantation is used in fabrication and can introduce defects into the material, it is important to understand deformation processes in defective Ge.

One means to address this question is to introduce defects into Ge by the technique of ion implantation, whereby a high-purity beam of monoenergetic ions is scanned across a target specimen and atomic displacements in the Ge matrix are created by the nuclear stopping process, leading to disordering and the build up of defects with ion fluence. The nature and extent of the radiation-induced damage in the specimen by the ion beam is dependent on the ion species, ion energy, fluence of ions, and the temperature at which implantation is carried out, all parameters that can be controlled precisely. A range of point defect distributions can be achieved without chemical modification by means of self-implantation, e.g., Ge ions into Ge. Thermal annealing after ion implantation induces the formation of extended defects, including large defect clusters and dislocation loops.[19]

In this study ion-implanted c-Ge specimens are prepared and the nanoindentation response investigated. Surprisingly, the implanted specimens are found to be significantly mechanically softer than pristine Ge. The evolution of implanted defects after thermal annealing is examined by transmission electron microscopy (TEM) and positron-annihilation spectroscopy (PAS), and compared with the nanoindentation response. The indent morphology is examined by TEM and atomic force microscopy (AFM). An explanation of the observed softening and thermal recovery is presented in the discussion.

 ©2009 The American Physical Society

II. EXPERIMENTAL DETAILS

Undoped single-crystal Ge(100) wafers (Wafer World, West Palm Beach) were implanted with 800 keV Ge ions at room temperature, using the ANU 1.7 MV NEC tandem accelerator. Specimens examined in the study were implanted with fluences of 3×10^{12}, 1×10^{13}, and 3×10^{13} ions$\cdot$cm^{-2} to create a damaged layer extending from the surface to a depth of up to ~700 nm. Ion damage profiles were simulated using the SRIM software package,[20] which uses Monte Carlo simulation of ion stopping. For this implant energy, a fluence of 1×10^{14} ions$\cdot$cm^{-2} or higher renders the surface of the c-Ge amorphous. Observations from ion-implanted amorphous Ge (a-Ge) specimens will be described in detail in a separate paper.

Some specimens were thermally annealed following implantation. Annealing was carried out in a quartz tube furnace under flowing argon. Specimens were annealed for 30 min at a constant temperature of either 150, 200, or 300 °C.

PAS was carried out to obtain information on open-volume defects generated by implantation, thereby giving an indication of the density of point defects created during the implantation as well as residual defects following the annealing step. Doppler broadening measurements of the 511-keV annihilation line were taken using a variable-energy positron beam (University of Western Ontario). The line-shape "*S*" parameter was used to characterize broadening.[21]

To investigate the mechanical properties of the implanted layer, specimens were indented with a UMIS-2000 nanoindenter (CSIRO, Australia) using a spherical diamond tip ($R \approx 4.3$ μm). Maximum loads of up to 100 mN were used. Load was applied in a single cycle with no hold period, using loading and unloading rates of ~1 mN$\cdot$s^{-1}. Hardness and Young's elastic modulus values shown were extracted using Oliver and Pharr's analysis[22] from tests made to 50 mN. This maximum load was used for hardness measurements because it was found to produce a well-developed plastic impression without appreciable cracking in all specimens.

Atomic force microscopy was carried out using a Quesant AFM in contact mode to examine the morphology of indents made in the implanted specimens. Additional AFM was done with a Digital Instruments Nanoscope III SPM.

Raman spectra were obtained from indents with a Renishaw 2000 Raman microscope, using the 632.8 nm line of a HeNe laser. The laser power was kept low to avoid annealing any metastable phases.[9] These measurements provided information on the structural phase present in the residual indent.

Indents were cross sectioned for TEM examination using an xT Nova NanoLab 200 dual-beam focused-ion-beam (FIB) system by the "lift-out" technique.[23] To prevent ion-beam damage to the region of interest specimens were coated with gold prior to insertion, and with platinum inside the FIB. TEM was performed using a Philips CM 300 operating at 300 keV.

III. RESULTS

Results from the SRIM simulation for vacancy production as a function of depth are shown in Fig. 1(a). The simulation predicts a damaged layer extending ~700 nm beneath the surface, increasing somewhat with fluence. This agrees with the cross-sectional TEM (XTEM) images shown in Figs. 1(b) and 1(c), where the implanted layer is visible, and clearly increases in depth with increasing fluence. Diffraction studies from the implanted layers showed no obvious evidence of the presence of an amorphous phase.

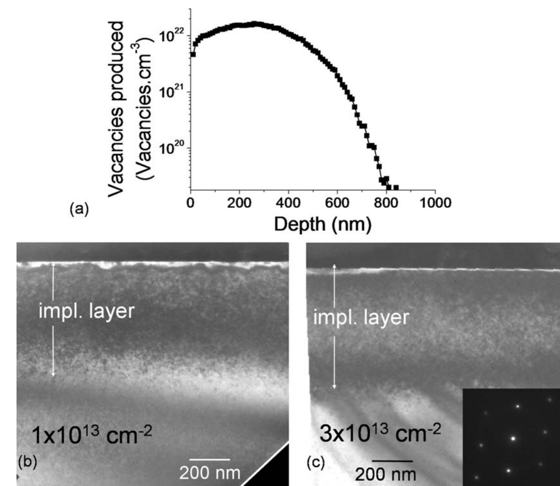

FIG. 1. (a) Vacancies produced as a function of depth for 3×10^{13} ions$\cdot$cm^{-2} Ge ions implanted into Ge at 800 keV, taken from SRIM simulations. The real vacancy concentration may be lower due to dynamic annealing. (b) Bright-field (BF) XTEM of implanted layer for 1×10^{13} ions$\cdot$cm^{-2} fluence. (c) BF XTEM of implanted layer for 3×10^{13} ions$\cdot$cm^{-2} fluence, with selected area diffraction pattern (SADP) from implanted layer inset.

Hardness values were calculated from nanoindentation *P-h* curves for both as-implanted and 200 °C annealed samples, as well as unimplanted Ge. The effects of ion implantation on the mechanical hardness of Ge are shown in Fig. 2, clearly illustrating the difference in mechanical response between implanted Ge and defect-free Ge. The measured hardness of the lowest-fluence as-implanted sample is equal to that of unimplanted Ge, at ~10.7 GPa. Hardness decreases for the 1×10^{13} ions$\cdot$cm^{-2} fluence specimen, and falls further still for the 3×10^{13} ions$\cdot$cm^{-2} specimen to ~9.0 GPa. After 200 °C annealing, hardness increases for all specimens to a fluence-independent value of ~11.1 GPa,

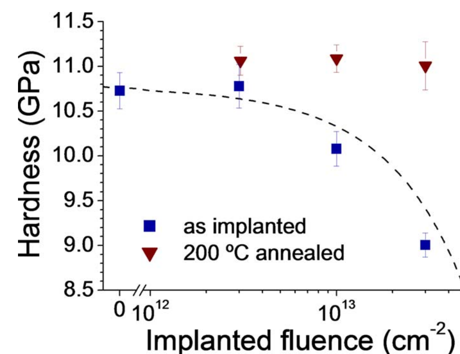

FIG. 2. (Color online) Indentation hardness versus implanted fluence, for as-implanted Ge specimens and for specimens postannealed at 200 °C. Dotted line: predicted hardness based on vacancy dependence [Eq. (5)].

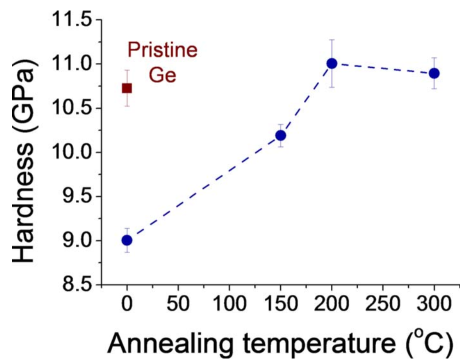

FIG. 3. (Color online) Hardness versus postimplant annealing temperature for Ge specimens implanted to a fluence of 3×10^{13} ions·cm^{-2}.

somewhat above the unimplanted value of 10.7 GPa. By contrast, the hardness of implanted a-Ge was measured and found to be ~7.6 GPa. We note that for the load of 50 mN used for hardness measurements the maximum penetration was ~300 nm, or ~40% of the implanted layer depth; thus there may be some substrate influence on the measured hardness. Hardness values from indents to 100 mN for the as-implanted samples were close to that of pristine Ge, indicating a more pronounced effect of the undamaged underlying material.

Hardness is shown as a function of annealing temperature in Fig. 3 for a set of specimens implanted to 3×10^{13} ions·cm^{-2}. Annealing at 150 °C partially recovers the hardness to its pristine value; annealing at 200 °C increases it further, to above the pristine value. Above 200 °C the hardness appears to plateau.

Elastic stiffnesses extracted from P-h curves were also found to differ markedly between implanted Ge and defect-free Ge. Young's modulus as a function of implanted fluence is plotted in Fig. 4. The Young's modulus exhibits a fluence-dependent decrease after implantation qualitatively similar to that for hardness. As with the hardness, the Young's modulus recovers to the pristine value after a 200 °C anneal.

AFM observations of residual indents provide complementary evidence of the difference in mechanical response of defective implanted Ge relative to defect-free Ge. A sharp

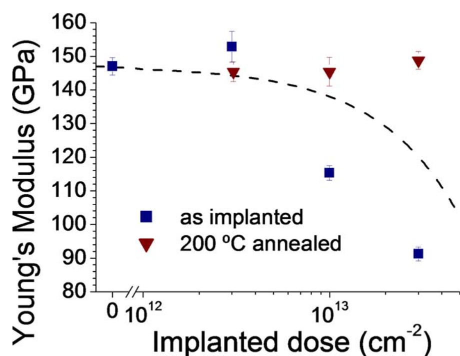

FIG. 4. (Color online) Young's modulus versus implanted fluence, for as-implanted specimens and specimens annealed at 200 °C. Dotted line: predicted modulus from vacancy fraction [Eq. (6)].

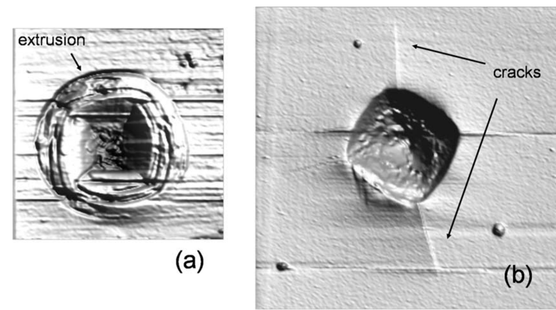

FIG. 5. AFM micrographs of indents to 100 mN in (a) Ge implanted to 3×10^{13} ions·cm^{-2} (unannealed), 7×7 μm image, and (b) unimplanted Ge, 10×10 μm image.

change is observed in the deformation morphology of samples after implantation to 1×10^{13} and 3×10^{13} ions·cm^{-2}. Figure 5(a) shows an indent to 100 mN in the 3×10^{13} ions·cm^{-2} as-implanted specimen. Indents in this specimen underwent considerable pile-up, featuring a ring of extruded material around the contact impression. Note that the horizontal straight lines in Fig. 5(a) are an artifact of AFM scanning. Similar pile-up around the impression was observed for indents in the 1×10^{13} ions·cm^{-2} as-implanted specimen. For comparison, Fig. 5(b) shows an indent to 100 mN in unimplanted Ge, exhibiting a typical brittle response with minimal uplift around the impression and radial cracks emanating from the edges. A similar brittle-type indent morphology was observed for the lowest-fluence (3×10^{12} ions·cm^{-2}) specimen, and also for indents in 200 °C annealed specimens for all fluences.

Raman microspectroscopy confirmed the crystalline structure of the implanted samples. Raman spectra from 3×10^{12} ions·cm^{-2} and 1×10^{13} ions·cm^{-2} fluence samples were identical to the spectrum of unimplanted Ge. The spectrum from the 3×10^{13} ions·cm^{-2} fluence as-implanted sample was similar, but featured a slight asymmetric shoulder on the low-energy side of the Ge-I peak. This feature disappeared after annealing at 200 °C. Raman spectroscopy showed that the changes in indent morphology were not accompanied by an indentation-induced phase transition, as has been previously observed for Ge under certain indentation conditions.[8,9] Raman spectra from indents in all the specimens examined contained only a single band at ~307 cm^{-1} corresponding to Ge-I, broadened and shifted due to residual compressive stresses.[6] This is shown in Fig. 6.

PAS supplied more detailed information on the structural state of implanted specimens. In Fig. 7(a), results of the PAS measurements are shown for specimens at different fluences, both as-implanted and annealed at 200 °C. The S parameter is plotted against incident positron energy. Estimated average positron penetration depth $\bar{z}$ is marked on the upper axis, calculated using the empirical formula[24]

$$\bar{z} = \frac{4.0\ \mu\text{g}\cdot\text{cm}^{-3}}{\rho_{\text{Ge}}} E^{1.6} \tag{1}$$

where E is positron energy in keV and $\rho_{\text{Ge}} = 5.324\ \text{g}\cdot\text{cm}^{-3}$. As-implanted specimens feature a fluence-

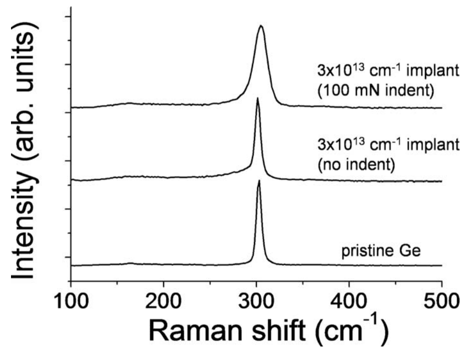

FIG. 6. Raman spectra collected from unimplanted Ge, as-implanted 3×10^{13} ions·cm^{-2} specimen, and an indent to 100 mN in the as-implanted 3×10^{13} ions·cm^{-2} specimen.

independent profile, with a peak value of approximately 0.50 ($S/S_{bulk}\approx1.033$). The similarity of the profiles can be attributed to saturated positron trapping due to the high concentration of implantation-induced point defects. Specimens annealed at 200 °C have a higher S parameter, peaking at about 0.51–0.515 ($S/S_{bulk}\approx1.054-1.064$), indicating an evolution to a lower concentration of larger open-volume defects.

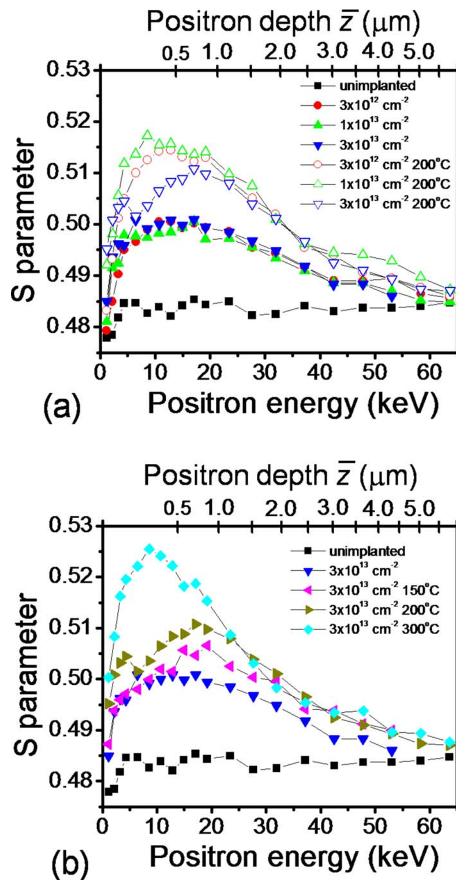

FIG. 7. (Color online) PAS results: (a) Doppler broadening S parameter as a function of incident positron energy for pristine, as-implanted, and 200 °C-annealed specimen. (b) S parameter versus positron energy for 3×10^{13} ions·cm^{-2} implanted specimen annealed at a range of temperatures. Estimated average penetration depth is shown on the upper axis.

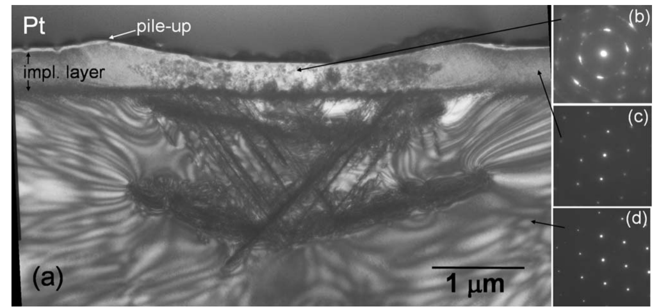

FIG. 8. (a) BF XTEM micrograph showing indent to 100 mN in 3×10^{13} ions·cm^{-2} as-implanted specimen, (b) SADP from deformed layer, (c) SADP from implanted layer outside deformed region, (d) SADP from pristine crystal.

Figure 7(b) shows PAS results for a range of postimplantation annealing temperatures. S parameter increases with increasing annealing temperature, reaching a peak of ~0.525 ($S/S_{bulk}\approx1.085$) for the 300 °C-annealed specimen.

XTEM was used to examine plastic deformation after indentation for individual indents. XTEM micrograph Fig. 8(a) shows plastic deformation in the as-implanted 3×10^{13} ions·cm^{-2} specimen after indentation to 100 mN. Contrast associated with deformation within the implanted layer cannot be clearly discerned, with no clear slip bands or twins. The SADP taken from within the deformed layer [Fig. 8(b)] shows a pattern characteristic of Ge-I, with some circular streaking that may be indicative of local lattice rotations within the deformed region. These features are not observed from the implanted layer outside the deformed region [Fig. 8(c)]. Pile-up is apparent at the edges of the impression. Below the implanted layer, the indentation damage is closer to that observed in bulk Ge,[7] with sharply defined slip and twin bands along 111 planes and a region of punched-out defects ~1 and ~2 μm below the surface.

Figure 9(a) shows plastic deformation in the 200 °C-annealed specimen. The damage layer clearly visible in the as-implanted material is no longer readily apparent, although PAS measurements confirmed the presence of residual defects in the layer following annealing at 200 °C. High resolution TEM would probably be required to observe these postannealing defects. The shear damage in the specimen resembles that in bulk Ge, that is, slip bands and twins

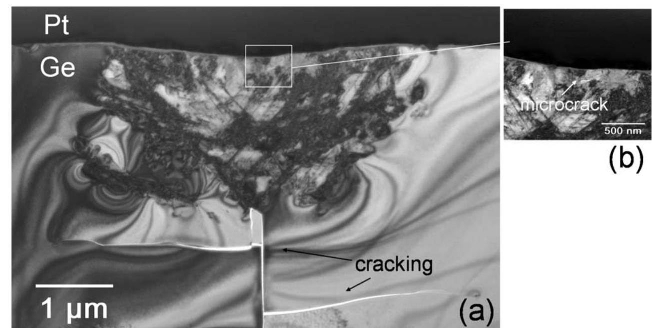

FIG. 9. (a) BF XTEM of indent to 100 mN in 3×10^{13} ions·cm^{-2} 200 °C-annealed specimen, (b) magnified view of microcrack within deformed region.

along {111} planes. Notably, though, cracking under the indent is extensive. A median crack runs from the bottom of the plastic zone, with lateral cracks branching off on either side. Moreover, voids and microcracks are present within the plastic zone, as shown more clearly in the higher-magnification view in Fig. 9(b). Similar extensive cracking was observed in other XTEM indent cross sections from the annealed specimen.

IV. DISCUSSION

The hardnesses measured for the higher fluence as-implanted layers indicate that the implanted material has a lower resistance to plastic flow than pristine Ge. This softening manifests in pronounced extrusion around indents [Fig. 5(a)]. The softer implanted layer is constrained by the harder undamaged Ge beneath and is pushed to the edges of the contact periphery during indentation. Plastic extrusion was most pronounced for indents loaded to 100 mN, for which the influence of the underlying material was greatest, but extrusion was also observed for indents to 50 mN. Cracking is suppressed up to 100 mN, likely because plastic flow acts as a more favorable means of relieving strain.

Mechanical softening at a high defect concentration is contrary to experience with many materials, particularly metals, in which crystal defects are generally associated with strengthening.[14,15] In metals, the chief barrier to slip is the presence of existing defects, and hardness may vary over orders of magnitude for high and low defect densities. In covalent semiconductors, however, hardness is a more intrinsic property governed by the energy of breaking and reforming chemical bonds,[16] and the main barrier to defect motion and slip is the high Peierls stress in these materials.[25,26]

A possible explanation for the softening is that there are nanosized pockets of amorphous material present within the implanted layer. Since a-Ge is softer than c-Ge, the total hardness would be reduced. Although ion-implanted continuous amorphous layers in Ge recrystallize by solid-phase epitaxy at temperatures of 300–400 °C,[27] isolated small amorphous zones may recrystallize at much lower temperatures,[28] so this scenario is not necessarily inconsistent with the hardness recovery after annealing. The fraction of amorphous material needed to produce the observed softening can be estimated. A simple composite model for an evenly distributed two-phase material predicts a hardness of

$$H_{av} = f_{cGe} H_{cGe} + f_{aGe} H_{aGe}, \quad (2)$$

where H_{av} is the composite hardness, and f_x and H_x are the volume fraction and hardness respectively of each phase.[29] Using the measured hardnesses in Fig. 2, and a hardness for a-Ge of H_{aGe}=7.6 GPa, the composite model predicts an amorphous volume fraction of f_{aGe}=0.2 for the 1×10^{13} ions$\cdot$cm^{-2} specimen and f_{aGe}=0.55 for the 3×10^{13} ions$\cdot$cm^{-2} specimen. Volume fractions of 20% and 55% a-Ge seem improbable. One would expect such high concentrations to be prominent in both TEM and Raman measurements, but a-Ge was not observed by either technique, suggesting that pockets of a-Ge are not responsible for the changes in mechanical properties observed here.

A more likely cause of the softening is the large number of point defects and small defect clusters, and correspondingly high density of dangling bonds, that are created by ion implantation. We propose that this high dangling-bond density may aid the motion of dislocations. Dislocation mobility in Ge has been found to be controlled by the formation and motion of kinks along the dislocation line,[26,30–32] processes that in pristine crystal can only occur by the breaking of covalent atomic bonds. It may be that the presence of preexisting dangling bonds lowers the barrier to kink mobility by relaxing the requirement for bond breaking. This would facilitate dislocation motion, therefore enhancing plastic flow.

Another way to view the softening effect is to regard vacancies as ‘missing bonds’ that reduce the strength of the material. Gao *et al.* have shown that hardness is proportional to the density of atomic bond strength for a covalent solid,[16] and hardness has been found to be lowered in the presence of high vacancy concentrations in other materials.[33,34] Gao *et al.* offer the following relationship for hardness:

$$H = AN_a E_g = AN_B^{2/3} E_g, \quad (3)$$

where E_g is the band gap, N_a is covalent bond number per unit area, N_B is the density of covalent bonds per unit volume, and A is a proportionality coefficient. Vacancies will lower the bond density to $N_{Bv}=(1-f_v)N_{B0}$, where f_v is the fractional vacancy concentration and N_{B0} is the bond density of the pristine material. The hardness with vacancies present will then be proportionally reduced to

$$H_v = H_{cGe}(1-f_v)^{2/3}, \quad (4)$$

where H_{cGe} is the hardness of pristine material. Vacancy production during implantation is proportional to fluence. The SRIM calculation gives an average vacancy production rate over the ~700 nm implanted layer of 3.074 vacancies/Å/ion. For Ge with an atomic density of 5.00×10^{23} atoms$\cdot$cm^{-3}, this gives a fractional vacancy concentration of $f_v=6.1\times10^{-15}F$, where F is the implanted fluence in ions$\cdot$cm^{-2}. Inserting this into Eq. (4) gives a fluence dependence for the hardness of

$$H = H_{cGe} \times (1 - 6.1\times10^{-15}F)^{2/3}. \quad (5)$$

This relationship is plotted against the measured hardness values as a function of fluence in Fig. 2. Although this approach ignores potentially important factors such as dynamic defect recombination and the presence of interstitials, it appears to give reasonably good agreement with the measured values. This suggests that the fraction of intact bonds is a useful way of looking at the effect of implantation damage on the hardness response.

An alternative possibility is that the increased free volume in the material due to high vacancy concentrations facilitates deformation, similar to the free volume-mediated, nonvolume-conserving deformation processes that are responsible for shear deformation in glassy systems.[35–37] The processes of free volume creation and annhilation thought to give rise to shear banding in glasses are dependent upon the random amorphous arrangement of atoms and continuous distribution of void sizes present in glasses,[35] and are not

directly applicable to covalently bonded crystalline Ge. However, the high level of disorder generated by ion implantation in Ge may result in Ge behaving more like a glassy metal. In any case, directed vacancy diffusion under the influence of stress is a possible (volume-conserving) strain mechanism even in covalent crystalline material if it is highly defective. It is difficult to evaluate the contribution of such a diffusion-based mechanism, which will be highly sensitive to the energy barrier to vacancy motion (higher in covalent than in metallic glassy systems). Finally, we note that the high density of plastic damage visible in TEM (Fig. 8) implies that a defect-related mechanism such as dislocation slip is acting.

The decrease in Young's modulus in implanted samples is intriguing (Fig. 4), given that elastic modulus is often considered an intrinsic property largely independent of defect state.[14] However this observation is consistent with previous reports that a high vacancy concentration can lower elastic modulus in covalent materials.[33,34] The elastic modulus of a material is proportional to the stiffness of the atomic bonds in the material. The change in modulus can be modeled as a reduction proportional to the fraction of bonds removed,

$$E = E_{\mathrm{cGe}}(1 - f_{\mathrm{v}}) = E_{\mathrm{cGe}} \times (1 - 6.1 \times 10^{-15} F). \qquad (6)$$

This relation is plotted in Fig. 4 and it appears to match the qualitative behavior of the measured elastic modulus with implanted fluence quite well. However, the quantitative agreement is not as good as is the relationship for hardness.

Postimplantation thermal annealing has the effect of repairing dangling bonds and causes simple vacancy-type and interstitial-type defects to recombine and annihilate, or to coalesce to form line defects (dislocations) and other extended defects.[19,38,39] The removal of vacancies and dangling bonds would be expected to remove the softening effect, which is exactly what was observed (Fig. 3). In fact, after 200 °C annealing the implanted specimens were harder than pristine Ge. This indicates that the extended defect structures present an impediment to plasticity and can be attributed to dislocation pinning, similar to the work hardening effect observed during indentation of pristine Ge.[7]

Compared to Ge, Si has been found to exhibit a much smaller change in mechanical properties after nonamorphising ion implantation. Williams *et al.* looked at the indentation response of Si implanted to high fluences and observed only a small decrease in hardness.[40] One explanation for this is that, in contrast to Ge under the conditions studied, the hardness of Si is mainly controlled by a pressure-induced phase transformation[11,41] rather than shear plasticity. Presumably the presence of implantation damage has minimal effect on the threshold stress for the phase transformation.

The PAS results in Fig. 7 show that a high density of open-volume defects are generated by ion implantation. The Doppler broadening S parameter value for the as-implanted specimens is $S/S_{bulk} \approx 1.033$. This low value may indicate the presence of simple vacancy-type defects, such as the divacancy or vacancy-impurity pairs.[38] For annealed specimens, the S parameter increases. Theoretical calculations and experiments for Si have shown that higher S parameter values correspond to larger vacancy clusters.[42,43] A similar trend can be expected for Ge. Below the saturation limit ($\sim 10^{15}$ cm^{-3}) however the S parameter is also sensitive to the number of defects,[44] so it must be interpreted with care. The S parameter rises after 200 °C annealing, and still further after 300 °C annealing. Since annealing is unlikely to increase the total number of defects, the increase in S can be attributed to the formation of larger defects. Annealing causes smaller vacancy-type defects to coalesce to form larger vacancy clusters. Other studies have similarly found that irradiation-induced vacancies in Ge become mobile at 200 °C and form larger vacancy clusters.[38,39] Interstital-type defects cannot be observed by PAS, but other studies have found that they show similar annealing behavior.[45]

The PAS information can be used to estimate a lower bound on the vacancy concentration in the as-implanted specimens. Assuming the characteristic S value of the vacancies to be the measured (saturated) value of 1.033, the trapped fraction of positrons is given by

$$F = \frac{vC}{1/t + vC}, \qquad (7)$$

where v is the trapping rate for vacancies, t is the positron lifetime for Ge, and C is the fractional defect concentration. Taking v to have a typical value of 10^{15} s^{-1}, taking the lifetime for Ge to be 230 ps,[46] and assuming not less than 95% trapping, Eq. (7) gives a minimum vacancy concentration of $\sim 10^{19}$ cm^{-3}. This is consistent with the vacancy concentrations found by SRIM simulation. Carrying out implants at lower fluences would be valuable in order to measure defect introduction rates in Ge, which could be directly compared with the vacancy production rate used to calculate Eq. (5).

Interestingly, the annealing behavior of vacancies in Ge may be dependent on the electronic doping type of the material. For p-type or low-doped Ge (such as that used in this study) the divacancy defect is expected to have a neutral charge state; for n-type Ge divacancies are expected to be negatively charged, and will not coalesce to form larger defect clusters.[39] Therefore n-type Ge might not exhibit the same behavior observed here. Further measurements on n-type material would be valuable.

Finally, it is interesting that TEM shows considerable subsurface cracking for indents in the annealed specimen. Microcracks and voids are observed even within the central plastic zone, as shown in Fig. 9(b). Crack formation in this central indentation zone is normally suppressed by the highly compressive stresses found there during indentation.[47] Extensive cracking is also observed below the plastic zone. This unusually extensive cracking may be related to the vacancy clusters by PAS observed after annealing. These vacancy clusters may act as preferential nucleation sites for cracks, and may also acts as stress concentrators to aid crack growth.[48] Indeed, evidence suggests that vacancy clusters induced in silicon by hydrogen implantation act as crack nucleation sites[49] in the Smart Cut process used to produce silicon-on-insulator wafers.[50]

V. CONCLUSION

The nanoindentation response of ion-implanted c-Ge has been investigated. After high fluence ion implantation the

hardness of the material decreases significantly. Indent morphology is altered, with extrusion around residual impressions and an absence of cracking. This enhanced plasticity is attributable to disorder generated by ion implantation. We propose a high dangling-bond density reduces resistance to dislocation motion in the material. After a low-temperature thermal anneal the mechanical response is restored close to that of pristine material, with a slightly elevated hardness. We attribute this recovery to vacancy-interstitial recombination and the coalescence of simple defects into larger extended defects after annealing. This study thus demonstrates that the mechanical response of covalent materials is dependent on their defect state, not solely an intrinsic property of the material. Nonetheless, a description of the relative hardness in terms of vacancy concentration appears to provide good agreement with the data, supporting the notion that hardness is dependent on the density of covalent bonding. Further work is needed on other covalent materials, such as compound semiconductors, to determine if this implantation-induced mechanical softening is a general phenomenon.

ACKNOWLEDGMENT

The Australian Research Council is acknowledged for financial support.

*oliverd@physics.mcgill.ca

[1] S. Nakaharai, T. Tezuka, N. Sugiyama, Y. Moriyama, and S.-I. Takagi, Appl. Phys. Lett. **83**, 3516 (2003).
[2] Y. Liu, M. D. Deal, and J. D. Plummer, Appl. Phys. Lett. **84**, 2563 (2004).
[3] R. F. Cook, J. Mater. Sci. **41**, 841 (2006).
[4] G. M. Pharr, W. C. Oliver, R. F. Cook, P. D. Kirchner, M. C. Kroll, T. R. Dinger, and D. R. Clarke, J. Mater. Res. **7**, 961 (1992).
[5] S. J. Lloyd, J. M. Molina-Aldareguia, and W. J. Clegg, J. Mater. Res. **16**, 3347 (2001).
[6] Y. G. Gogotsi, V. Domnich, S. N. Dub, A. Kailer, and K. G. Nickel, J. Mater. Res. **15**, 871 (2000).
[7] J. E. Bradby, J. S. Williams, J. Wong-Leung, M. V. Swain, and P. Munroe, Appl. Phys. Lett. **80**, 2651 (2002).
[8] J. Jang, M. J. Lance, S. Wen, and G. M. Pharr, Appl. Phys. Lett. **86**, 131907 (2005).
[9] D. J. Oliver, J. E. Bradby, J. S. Williams, M. V. Swain, and P. Munroe, J. Appl. Phys. **101**, 043524 (2007).
[10] V. Domnich, Y. Gogotsi, and S. N. Dub, Appl. Phys. Lett. **76**, 2214 (2000).
[11] J. E. Bradby, J. S. Williams, J. Wong-Leung, M. V. Swain, and P. Munroe, Appl. Phys. Lett. **77**, 3749 (2000).
[12] J. E. Bradby, J. S. Williams, J. Wong-Leung, M. V. Swain, and P. Munroe, Appl. Phys. Lett. **78**, 3235 (2001).
[13] J. E. Bradby, S. O. Kucheyev, J. S. Williams, C. Jagadish, M. V. Swain, P. Munroe, and M. R. Phillips, Appl. Phys. Lett. **80**, 4537 (2002).
[14] T. H. Courtney, *Mechanical Behavior of Materials*, 2nd ed. (McGraw-Hill, Boston, 2000).
[15] D. Hull and D. J. Bacon, *Introduction to Dislocations*, 3rd ed. (Pergamon Press, Oxford, 1984).
[16] F. M. Gao, J. L. He, E. D. Wu, S. M. Liu, D. L. Yu, D. C. Li, S. Y. Zhang, and Y. J. Tian, Phys. Rev. Lett. **91**, 015502 (2003).
[17] F. M. Gao, Phys. Rev. B **73**, 132104 (2006).
[18] A. Simunek and J. Vackar, Phys. Rev. Lett. **96**, 085501 (2006).
[19] J. W. Corbett, J. P. Karins, and T. Y. Tan, Nucl. Instrum. Methods Phys. Res. **182-183**, 457 (1981).
[20] J. F. Ziegler, www.srim.org
[21] P. Asoka-Kumar, K. G. Lynn, and D. O. Welch, J. Appl. Phys. **76**, 4935 (1994).
[22] W. Oliver and G. Pharr, J. Mater. Res. **7**, 1564 (1992).
[23] R. M. Langford and A. K. Petford-Long, J. Vac. Sci. Technol. A **19**, 2186 (2001).
[24] A. Vehanen, K. Saarinen, P. Hautojärvi, and H. Huomo, Phys. Rev. B **35**, 4606 (1987).
[25] H. Alexander and P. Haasen, Solid State Phys. **22**, 27 (1968).
[26] A. George and J. Rabier, Rev. Phys. Appl. **22**, 941 (1987).
[27] E. P. Donovan, F. Spaepen, D. Turnbull, J. M. Poate, and D. C. Jacobson, J. Appl. Phys. **57**, 1795 (1985).
[28] S. E. Donnelly, R. C. Birtcher, V. M. Vishnyakov, and G. Carter, Appl. Phys. Lett. **82**, 1860 (2003).
[29] R. Hill, Proc. Phys. Soc., London, Sect. A **65**, 349 (1952).
[30] J. J. Gilman, Science **261**, 1436 (1993).
[31] H. R. Kolar, J. C. H. Spence, and H. Alexander, Phys. Rev. Lett. **77**, 4031 (1996).
[32] Y. L. Iunin, V. I. Nikitenko, V. I. Orlov, and B. V. Petukhov, Phys. Rev. Lett. **78**, 3137 (1997).
[33] X. Jiang, M. Wang, K. Schmidt, E. Dunlop, J. Haupt, and W. Gissler, J. Appl. Phys. **69**, 3053 (1991).
[34] S.-H. Jhi, S. G. Louie, M. L. Cohen, and J. Ihm, Phys. Rev. Lett. **86**, 3348 (2001).
[35] F. Spaepen, Acta Metall. **25**, 407 (1977).
[36] J. T. Hagan, J. Mater. Sci. **15**, 1417 (1980).
[37] C. A. Schuh, T. C. Hufnagel, and U. Ramamurty, Acta Mater. **55**, 4067 (2007).
[38] A. Peaker, V. Markevich, L. Murin, N. Abrosimov, and V. Litvinov, Mater. Sci. Eng., B **124-125**, 166 (2005).
[39] K. Kuitunen, F. Tuomisto, J. Slotte, and I. Capan, Phys. Rev. B **78**, 033202 (2008).
[40] J. S. Williams, Y. Chen, J. Wong-Leung, A. Kerr, and M. V. Swain, J. Mater. Res. **14**, 2338 (1999).
[41] D. R. Clarke, M. C. Kroll, P. D. Kirchner, R. F. Cook, and B. J. Hockey, Phys. Rev. Lett. **60**, 2156 (1988).
[42] H. Kauppinen, C. Corbel, K. Skog, K. Saarinen, T. Laine, P. Hautojärvi, P. Desgardin, and E. Ntsoenzok, Phys. Rev. B **55**, 9598 (1997).
[43] M. Hakala, M. J. Puska, and R. M. Nieminen, Phys. Rev. B **57**, 7621 (1998).
[44] S. Ruffell, P. J. Simpson, and A. P. Knights, J. Phys.: Condens. Matter **19**, 466202 (2007).
[45] V. Markevich, A. Peaker, A. Markevich, V. Litvinov, L. Murin, and V. Emtsev, Mater. Sci. Semicond. Process. **9**, 613 (2006).

[46] A. Polity and F. Rudolf, Phys. Rev. B **59**, 10025 (1999).
[47] S. S. Chiang, D. B. Marshall, and A. G. Evans, J. Appl. Phys. **53**, 298 (1982).
[48] B. R. Lawn, *Fracture of Brittle Solids*, 2nd ed. (Cambridge University Press, Cambridge, 1993).
[49] O. Moutanabbir, B. Terreault, M. Chicoine, F. Schiettekatte, and P. J. Simpson, Phys. Rev. B **75**, 075201 (2007).
[50] M. Bruel, Electron. Lett. **31**, 1201 (1995).